ADVANCED MATERIALS

Supporting Information

for *Adv. Mater.*, DOI: 10.1002/adma.202004515

Shape Programming by Modulating Actuation over Hierarchical Length Scales

*Tian Gao, Emmanuel Siéfert, Antonio DeSimone, and Benoît Roman**

Supporting Information

Shape Programming by Modulating Actuation over Hierarchical Length Scales

Tian Gao[1], Emmanuel Siéfert[1], Antonio DeSimone[2,3], and Benoît Roman[1*]

[1]PMMH, CNRS, ESPCI Paris, PSL University, Sorbonne Universités, Université de Paris, F-75005 Paris, France

[2]MathLab, SISSA-International School for Advanced Studies, 34136 Trieste, Italy

[3]The Biorobotics Institute and Department of Excellence in Robotics and AI, Scuola Superiore Sant'Anna, 56127 Pisa, Italy

**E-mail: benoit.roman@espci.fr*

Contents

1 Material characterization and actuation techniques

In the main manuscript, three responsive materials, recently presented in published work, are used in order to demonstrate the hierarchical zigzag patterning strategy. We here detail the fabrication, actuation of the materials and their characteristics succinctly presented in the experimental section.

1.1 Inflated fabrics

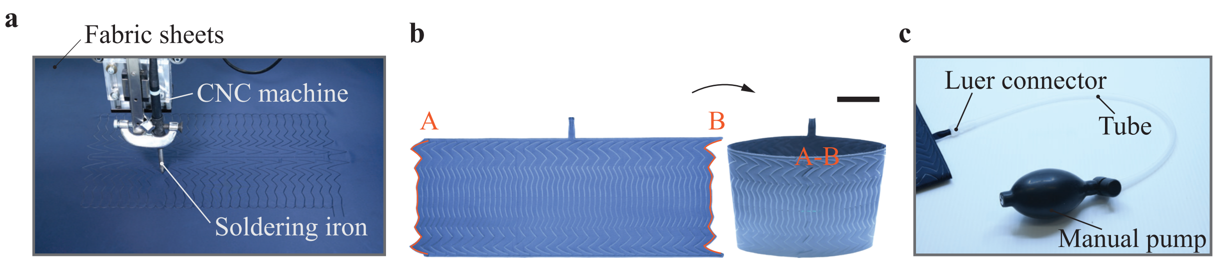

Figure S1: Inflated fabrics fabrication steps. (a) Two superimposed flat fabric sheets are sealed along a specific zigzag pattern with a soldering iron mounted on a CNC machine. (b) After cutting along its boundary, the flat structure is closed and glued onto a cylindrical shape. (c) The network of channels comprised between the two fabric sheets are connected to an inflating bulb via Luer connectors and a silicon tube. The typical applied pressure is 0.5 bar. Scale bar: 50 mm.

The inflated fabric structures are made of one-sided TPU-coated Nylon fabric sheets. Two different fabrics are used in this study: tafetta 70 den of thickness 0.17 mm and weight per unit surface 170 g/m^2 and Ripstop 20 den of thickness 0.1 mm and weight per unit surface 70 g/m^2. The equivalent Young modulus along the fibre direction is estimated at around $1.5.10^8$ Pa for both fabric sheets. A soldering iron mounted on a CNC machine and heated at $230°C$ is used to seal two superimposed flat fabric sheets along a specific zigzag pattern at 120 mm/min (**Figure S1**a). The sample is then cut along its boundary. Using a RS pro superglue gel, edge A and B are glued onto a cylindrical shape (Figure S1b). The structure is finally connected with Luer connectors and a silicon tube to an inflating bulb, in order to manually inflate the network of channels comprised between the two fabric sheets. The obtained shape does not depend on the applied pressure provided it is sufficiently high (to bend the fabric) [1]. The typical applied pressure is 0.5 bar (Figure S1c).

1.2 Mesostructured pneumatic elastomer (baromorphs)

In order to make baromorph structures, equal quantities of base and catalyst of vinylpoly-siloxane (VPS, Elite Double 8 from Zhermack, Young modulus of 250 kPa)

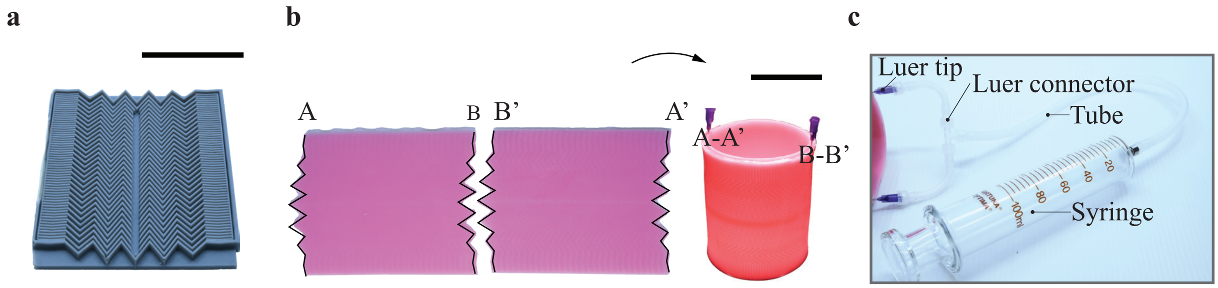

Figure S2: Baromorph fabrication steps. (a) 3D-printed mould containing a network of zigzag walls. (b) After casting and unmolding, a membrane made of the same material is glued to close the structures. Two structures are assembled along their boundaries and closed and glued onto a cylindrical shape. (c) The network of channels embedded in the elastomer structure is connected to a syringe via Luer connectors and a silicon tube. The typical applied pressure is 0.2 bar. Scale bar: 5 cm.

are mixed and cast in a 3D printed mold shown in **Figure S2**a. After curing (which typically takes $20min$ at room temperature) and unmolding, a membrane made of the same material is glued using uncured VPS to close the channels. Two identical flat structures are finally assembled along their boundaries (A-A’, B-B’) and glued onto a cylindrical shape using again uncured VPS mixture (Figure S2b).

In order to inflate the structure and trigger the shape transformation, the embedded channels are connected to a syringe via a silicon tube, Luer connectors and tips (Figure S2c). When pulling or pushing the syringe, the channels are respectively deflated and inflated, leading to contraction and expansion perpendicular to the channel direction. The typical applied pressure is 0.2 bar. More details may be found in ref. [2], as well as the theoretical model predicting the deformation as a function of pressure, channel geometry and density.

1.3 3D printed PLA

Following the work presented in Refs. [3, 4], we first calibrate the thermal contraction parallel and perpendicular to the printing direction as a function of the printed layer thickness. Plates (width w_0, length l_0) with different printed layer thicknesses t are thus printed (**Figure S3**a) with a Fused Filament Fabrication 3D-printer (Hyrel 16A, nozzle diameter 0.5 mm, PLA filament diameter 1.75 mm, bed temperature 42°C, nozzle temperature 200°C and printing speed 4000 mm/min, see **Figure S4**a). After printing, the samples are immersed in a bath of hot water (at 80°C) (Figure S4d) and deform to relax the flow-induced internal stresses. Contraction ratios $\lambda_\parallel = l/l_0$ and $\lambda_\perp = w/w_0$ are measured and plotted as a function of the extruded filament thickness. No significant perpendicular contraction $\lambda_\perp$ is observed whereas a monotonic correlation between $\lambda_\parallel$ and

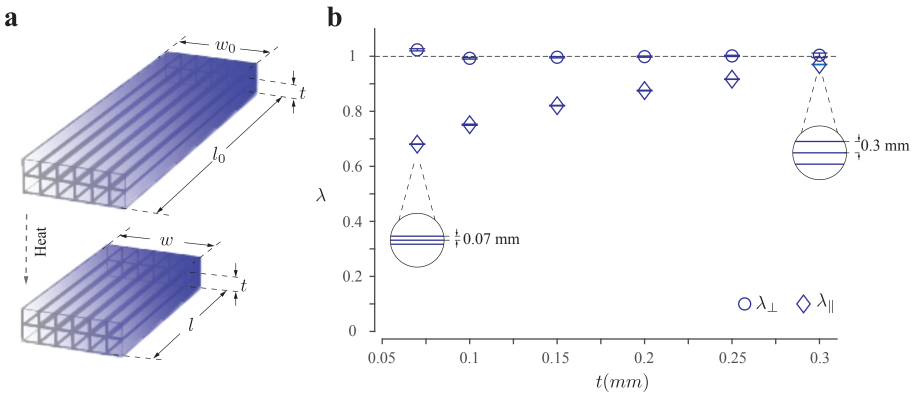

Figure S3: Actuation calibration of 3D printed filaments. (a) Plate (width w_0, length l_0) made of straight parallel extruded filaments of varying layer thicknesses t are 3D-printed along the long direction. After being inserted in a bath of hot water (at 80 °C), the plate shrinks anisotropically. (b) Measured contraction ratio $\lambda_\parallel$ and $\lambda_\perp$ as a function of the extruded filament thickness t (for a nozzle diameter of 0.5 mm).

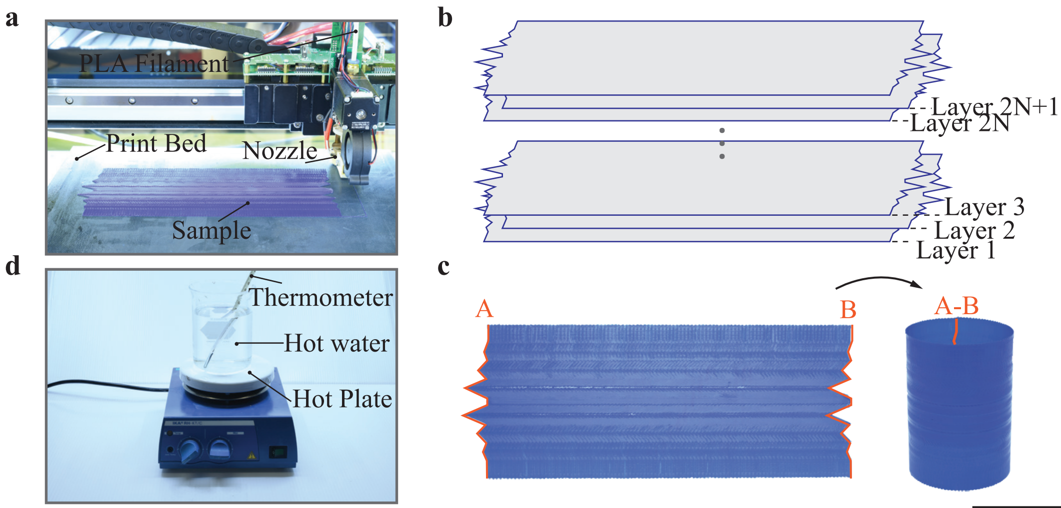

Figure S4: 3D-printed structure fabrication steps. (a) 3D-printing of the zigzag paths. (b) The sample is printed flat and is made of several layers, which are slightly offset to cover potential gaps in between the filaments. (c) The flat structure is then closed and glued onto a cylindrical shape. (d) The sample is then placed onto a hot water bath (80°) in order to trigger the metric change. Scale bar: 50 mm.

the layer thickness is observed (Figure S3b). Contraction ratios ranging from 0.68 to 0.97 may be obtained with this technique.

Zigzag structures are printed using the same printing parameters mentioned above. Even layers are slightly offset to cover potential gaps between the filaments (Figure S4b).

Once printed, the flat structure with varying zigzag angle is closed onto a cylindrical shape by heating edges A and B with a soldering iron at $200°C$ and assembling them (Figure S4c). When immersed in the hot water bath, the cylindrical structure morphs into a hyperbolic shape (see **Figure 4g** in the main manuscript).

2 Bisectrix construction and kinematic compatibility.

We show here that the interface between two regions with constant director $\boldsymbol{e}_\alpha$ and $\boldsymbol{e}_\beta$ leads to a kinematically compatible deformation if and only if the common line is one of the two bisectrices of the X-shaped cross formed by the lines parallel to $\boldsymbol{e}_\alpha$ and $\boldsymbol{e}_\beta$ (**Figure S5**)). In each patch the metric and its square root are given by

$$\begin{bmatrix} \lambda_\perp^2 & 0 \\ 0 & \lambda_\parallel^2 \end{bmatrix}, \quad g^{1/2} = \begin{bmatrix} \lambda_\perp & 0 \\ 0 & \lambda_\parallel \end{bmatrix} \tag{S1}$$

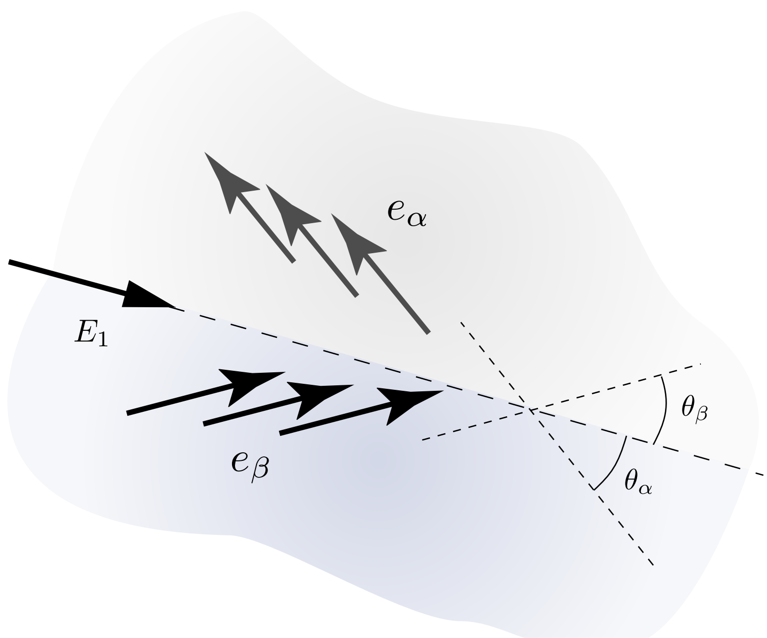

Figure S5: The active fields are kinematically compatible if the interface line is stretched by the same amount on both sides.

in the frame of reference aligned with the local direction of the director field. We denote $\lambda_\Sigma = \lambda_\parallel \lambda_\perp$ the area ratio change. Let us define $\boldsymbol{E}_1$ the vector tangent to the interface line and θ_α as the angle between $\boldsymbol{E}_1$ and $\boldsymbol{e}_\alpha$. Distances along this direction are stretched by a factor Λ_1, such that $\Lambda_1^2 = \boldsymbol{E}_1 \cdot g\, \boldsymbol{E}_1 = \lambda_\parallel^2 \cos^2\theta_\alpha + \lambda_\perp^2 \sin^2\theta_\alpha$

A combination of patches is kinematically compatible only if the interface line (which belongs to both patches) is stretched by the same amount by the two adjacent patches. In other words, $\lambda_\parallel^2 \cos^2\theta_\alpha + \lambda_\perp^2 \sin^2\theta_\alpha = \lambda_\parallel^2 \cos^2\theta_\beta + \lambda_\perp^2 \sin^2\theta_\beta$. which leads to $(\lambda_\parallel^2 - \lambda_\perp^2)\cos^2\theta_\alpha = (\lambda_\parallel^2 - \lambda_\perp^2)\cos^2\theta_\beta$. If the metric is not isotropic ($\lambda_\parallel \neq \lambda_\perp$), this condition imposes that the angles follow

$$\theta_\alpha = -\theta_\beta \equiv \theta_0$$

We conclude that the interface must be aligned with the bisectrix of the director fields, and denote by θ_0 the angle between the directors and the interface. Moreover,

$$|g^{1/2}(\pm\theta_0)\boldsymbol{E}_1| = (\boldsymbol{E}_1 \cdot g(\pm\theta_0)\boldsymbol{E}_1)^{1/2} = \Lambda_1 \tag{S2}$$

where

$$\Lambda_1 = \left(\lambda_\parallel^2 \cos^2\theta_0 + \lambda_\perp^2 \sin^2\theta_0\right)^{1/2}$$

and we have denoted with $g(\pm\theta_0)$ the metric tensor on the two sides of the interface, where the director before actuation is oriented parallel to either e_{θ_0} or $e_{-\theta_0}$.

Once Equation (S2) is satisfied, we can easily arrange that the deformations on the two sides of the interface, denoted by $F(\pm\theta_0)$, are such that $F(-\theta_0)\boldsymbol{E}_1 = F(\theta_0)\boldsymbol{E}_1$. This is the condition that guarantees that the interface (parallel to $\boldsymbol{E}_1$) is mapped to the same one line. In this case, $F(\pm\theta_0)$ are kinematically compatible in the sense that they define a piece-wise constant deformation that does not open discontinuities (fracture) across the interface. Indeed, by the polar decomposition theorem for tensors with positive determinant (see, e.g., [5]), $F(\pm\theta_0) = R^{(\pm)}g^{1/2}(\pm\theta_0)$, where $R^{(\pm)}$ are rotations. Therefore, for any $R^{(+)}$ (a global rotation that can be fixed arbitrarily), and since by (S2)

$$|R^{(+)}g^{1/2}(\theta_0)\boldsymbol{E}_1| = |g^{1/2}(-\theta_0)\boldsymbol{E}_1|$$

we can find a rotation $R^{(-)}$ so that $g^{1/2}(-\theta_0)\boldsymbol{E}_1$ can be rotated and brought to coincide with $R^{(+)}g^{1/2}(\theta_0)\boldsymbol{E}_1$. This is expressed by the formula

$$F(\theta_0)\boldsymbol{E}_1 = R^{(+)}g^{1/2}(\theta_0)\boldsymbol{E}_1 = R^{(-)}g^{1/2}(-\theta_0)\boldsymbol{E}_1 = F(-\theta_0)\boldsymbol{E}_1 \tag{S3}$$

whose geometric interpretation is illustrated in **Figure S6**.

The explicit calculation of deformations $F(\pm\theta_0)$ can be done with the help of a simple geometric construction. We now choose to work in the frame of reference $\mathbf{E}_1, \mathbf{E}_2$, and assume that direction $\mathbf{E}_1$ remains unchanged when the system is actuated. It is always possible to satisfy this condition by a rigid rotation of the whole system. The material points aligned with the director field e_{θ_0} are oriented after actuation with an angle θ (see **Figure S7**) with respect to $\mathbf{E}_1$. Simple geometry on the right-angle triangle in Figure S7 shows that $\tan\theta = (\lambda_\perp b)/(\lambda_\parallel a)$ so that

$$\tan\theta = \frac{\lambda_\perp}{\lambda_\parallel}\tan\theta_0 \tag{S4}$$

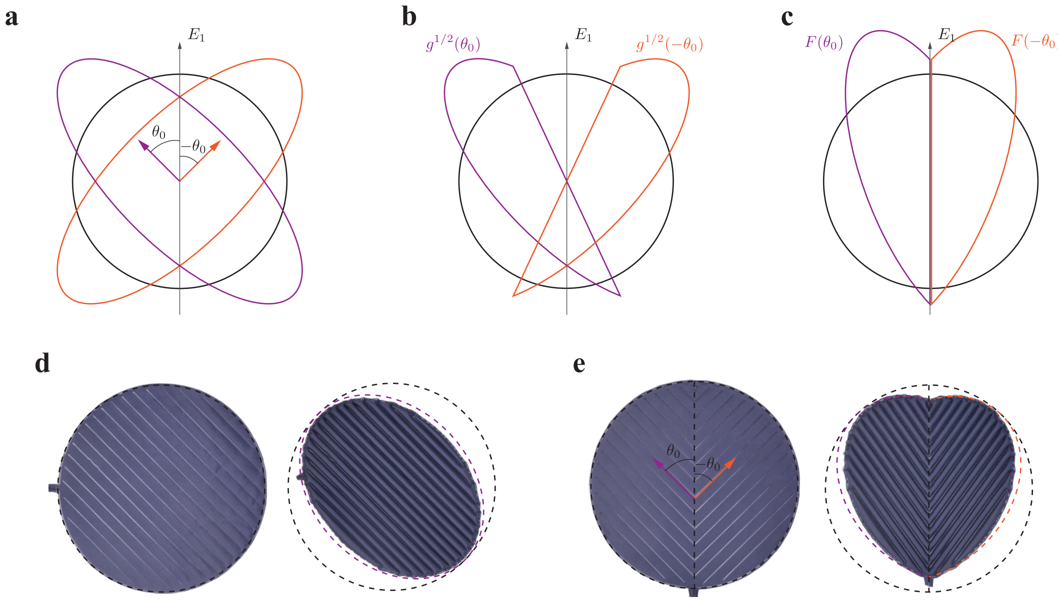

Figure S6: Geometric illustration of Equation (S3) **in the context of inflatable fabrics.** (a): a circular disk deformed by either $g^{1/2}(\theta_0)$ or $g^{1/2}(-\theta_0)$. (b): the left half of the disk is deformed by $g^{1/2}(\theta_0)$, the right one by $g^{1/2}(-\theta_0)$; this would require the opening of a discontinuity at the interface. (c): rigid rotations $R^{(\pm)}$ leave stretches unaffected on each side, and guarantee kinematic compatibility of the pair composed by $F(\theta_0) = R^{(+)}g^{1/2}(\theta_0)$ and $F(-\theta_0) = R^{(-)}g^{1/2}(-\theta_0)$ (continuity at the interface). (d): deformation $g^{1/2}(\theta_0)$ realized by inflatable fabrics (e): deformation induced by the kinematically compatible pair $F(\pm\theta_0)$ realized by inflatable fabrics

Actuation transforms $\mathbf{E}_1$ into $\Lambda_1\mathbf{E}_1$ and $\mathbf{e}_{\theta_0}$ into $\lambda_\parallel \mathbf{e}_\theta$, from which we deduce that $\mathbf{E}_2 = (\mathbf{e}_{\theta_0} - \cos\theta_0 \mathbf{E}_1)/\sin\theta_0$ is transformed into $(\lambda_\parallel \mathbf{e}_\theta - \Lambda_1 \cos\theta_0 \mathbf{E}_1)/\sin\theta_0$. We finally obtain the transformation as

$$F(\theta_0) = \begin{bmatrix} \Lambda_1 & (\lambda_\parallel \cos\theta - \Lambda_1 \cos\theta_0)/\sin\theta_0 \\ 0 & \lambda_\parallel \sin\theta/\sin\theta_0 \end{bmatrix} = \begin{bmatrix} \Lambda_1 & \frac{\lambda_\parallel^2 - \lambda_\perp^2}{2\Lambda_1} \sin 2\theta_0 \\ 0 & \Lambda_2 \end{bmatrix} \tag{S5}$$

where we have used the fact that $\sin\theta = \sin\theta_0 \lambda_\perp/\Lambda_1$, as inferred from geometry in Figure S7, and defined

$$\Lambda_2 = \lambda_\Sigma/\Lambda_1$$

Once $F(\theta_0)$ is known, $F(-\theta_0)$ is easily obtained by symmetry. Indeed, by Equation (S3), $F(-\theta_0)\boldsymbol{E}_1 = F(\theta_0)\boldsymbol{E}_1$ and hence the line parallel to $\boldsymbol{E}_1$ is left invariant by both $F(\pm\theta_0)$. The construction for the region of the zigzag where the director is initially oriented like $e_{-\theta_0}$ is easily obtained from the one illustrated in Figure S7 by a reflection across the interface line, which is parallel to $\boldsymbol{E}_1$. It follows that Equation (S5) is valid for both $\pm\theta_0$.

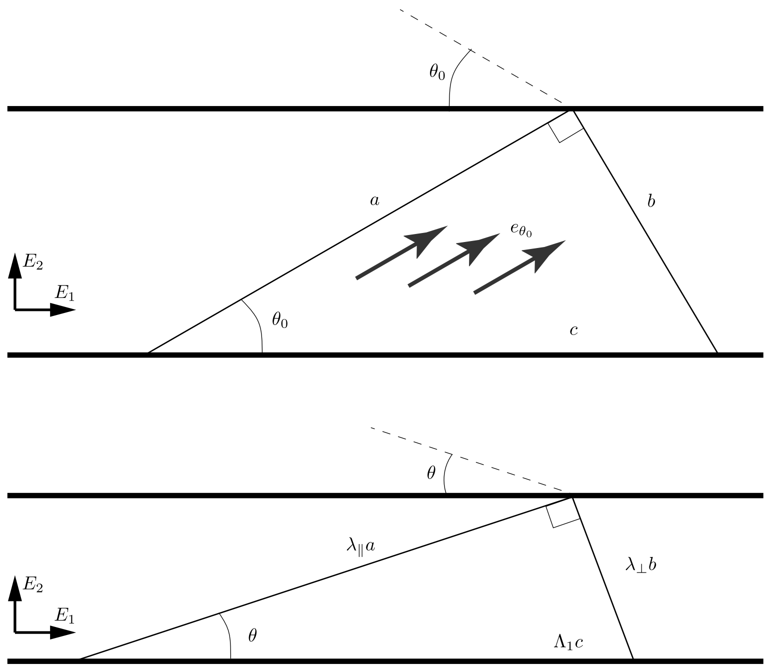

Figure S7: Geometric construction for an active patch with a director field oriented along $\mathbf{e}_{\theta_0}$ used for the calculation of the deformation $F(\theta_0) = R^{(+)}g^{1/2}(\theta_0)$. The material lines are drawn in the rest state (top) and in the actuated sate (bottom). The lines stay perpendicular since they are oriented along the principal directions of stretch (the eigenvectors of $g^{1/2}(\theta_0)$), which are both rotated by $R^{(+)}$ in the deformation $F(\theta_0) = R^{(+)}g^{1/2}(\theta_0)$.

3 Homogenized stretches (symmetric and asymmetric cases)

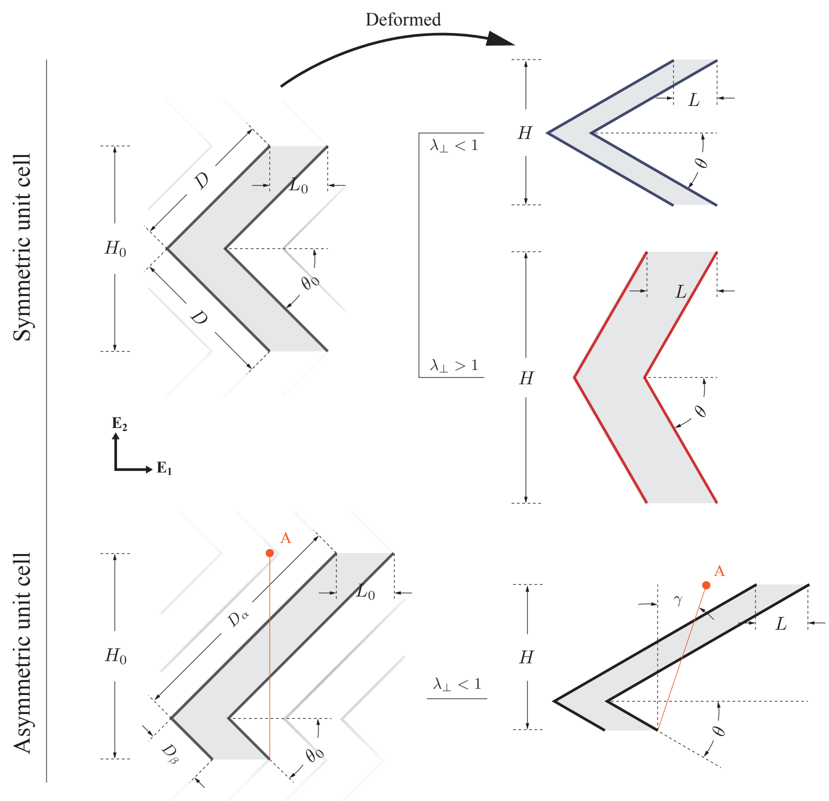

Figure S8: Geometry of the asymmetric (bottom) and symmetric (top, $D_\alpha = D_\beta = D$) zigzag unit cell, combining uniform director field (along thick marked lines), with interface along bisectrices. On the left, the reference state, and on the right, the deformed state.

In the $(\boldsymbol{E}_1, \boldsymbol{E}_2)$ frame of the interface/bisectrix (see **Figure S8**), the transformation induced by each the director field $F(\theta_0)$ and $F(-\theta_0)$ follow Equation (S5). When $F(\pm\theta_0)$ are combined in a zigzag pattern, the average transformation follows a simple mixing law :

$$\bar{F} = \frac{1}{1+\rho}F(\theta_0) + \frac{\rho}{1+\rho}F(-\theta_0) = \begin{bmatrix} \Lambda_1 & \frac{1-\rho}{1+\rho}\frac{\lambda_\parallel^2-\lambda_\perp^2}{2\Lambda_1}\sin 2\theta_0 \\ 0 & \Lambda_2 \end{bmatrix} = \begin{bmatrix} \Lambda_1 & \Lambda_2 \tan\gamma \\ 0 & \Lambda_2 \end{bmatrix} \quad \text{(S6)}$$

where $\rho = D_\beta/D_\alpha$, and we have identified the shearing angle γ from

$$\tan\gamma = \frac{1-\rho}{1+\rho}\frac{\lambda_\parallel^2 - \lambda_\perp^2}{2\lambda_\Sigma}\sin 2\theta_0$$

We recover in this expression the fact that for symmetric zigzag, $\rho = 1$, the shear angle is zero.

An interesting property of this transformation is that both diagonal terms are constant, and do not depend on the asymmetry parameter ρ. This means that the height H and the length L of a zigzag unit (such as in Figure S8) are always stretched by same factors (Λ_1, Λ_2), independently of asymmetry.

The metric $\bar{G} = \bar{F}^T \bar{F}$ is therefore

$$\bar{G} = \begin{bmatrix} \Lambda_1^2 & \lambda_\Sigma \tan\gamma \\ \lambda_\Sigma \tan\gamma & \Lambda_2^2(1+\tan^2\gamma) \end{bmatrix} \tag{S7}$$

4 Achievable stretches are always in the interval between $\lambda_\perp$ and $\lambda_\parallel$

We see that $\det \bar{G} = \Lambda_1^2 \Lambda_2^2 = \lambda_\Sigma^2$, so that the area change is always the same, independently of zigzag angle θ_0, but also on the asymmetry ρ.

We now show more rigorously that the eigenvalues of Equation (S7) always lie between $\lambda_\perp^2$ and $\lambda_\parallel^2$ or, equivalently, that the principal stretches always lie between $\lambda_\perp$ and $\lambda_\parallel$. This can be done by a direct calculation, but we provide a more geometric argument based on the notion of maximal stretch. In fact, since the principal stretches give the maximal possible extension or contraction along a material line, $\lambda_\perp$ and $\lambda_\parallel$ give a bound for the maximal extension and contraction that can be achieved by actuation with *any* zigzag construction, no matter what its geometric details are.

We denote by $\lambda_{max}(F)$ and $\lambda_{min}(F)$ the maximal and minimal principal stretches of the deformation F, defined as the maximum and minimum singular values of F or, equivalently, the square roots of the largest and smallest eigenvalues of $F^T F$. In view of the well known property

$$\lambda_{max}(F) = \sup\{|F\boldsymbol{e}| : |\boldsymbol{e}| = 1\} \tag{S8}$$

where the supremum is taken over all two-dimensional vectors of unit length, the function $F \mapsto \lambda_{max}(F)$ is convex (as the point-wise supremum of convex functions).

Therefore, recalling that $\bar{F} = \frac{1}{1+\rho}F(\theta_0) + \frac{\rho}{1+\rho}F(-\theta_0)$, convexity of $\lambda_{max}(F)$ implies

$$\lambda_{max}(\bar{F}) \leq \frac{1}{1+\rho}\lambda_{max}(F(\theta_0)) + \frac{\rho}{1+\rho}\lambda_{max}(F(-\theta_0)) = \lambda_{max}(g^{1/2}(\pm\theta_0)) \tag{S9}$$

where we have used that $\lambda_{max}(F(\theta_0)) = \lambda_{max}(F(-\theta_0)) = \lambda_{max}(g^{1/2}(\pm\theta_0))$.
Since $\lambda_{max}(g^{1/2}(\pm\theta_0))$ is contained in the interval between $\lambda_\perp$ and $\lambda_\parallel$, we have that $\lambda_{max}(\bar{F})$ cannot exceed the largest between $\lambda_\perp$ and $\lambda_\parallel$. Then, in view of the fact that $\lambda_{min}(\bar{F})\lambda_{max}(\bar{F}) = det^{1/2}(\bar{G}) = \lambda_\Sigma = \lambda_\perp\lambda_\parallel$, $\lambda_{min}(\bar{F})$ must be larger than the smallest between $\lambda_\perp$ and $\lambda_\parallel$. It then follows that both $\lambda_{max}(\bar{F})$ and $\lambda_{min}(\bar{F})$ are contained in the interval between $\lambda_\perp$ and $\lambda_\parallel$.

5 Deformations achieved with asymmetric zigzags can be obtained by rotating the ones achieved with symmetric zigzags

We have found that every non-symmetric zigzag generates a metric $\bar{G}$ that can also be obtained using a symmetric zigzag, with a different internal angle, and with rotated bisectrix direction. We illustrate this by considering inflatable fabric zigzag cells with a fixed internal angle $\theta_0 = 45°$, but a varying asymmetry parameter ρ. The eigenvalues of the metric $\bar{G}$ from Equation (S7) provide the principal stretches(**Figure S9** center), and we do observe that they lie in the range $[\lambda_\perp = 0.73 \quad 1 = \lambda_\parallel]$. The equivalent symmetric zigzag pattern is the one that has the same principal stretches. The internal angle θ_0' of this symmetric zigzag is obtained by inverting Equation (2) from the main text (see Figure S9 bottom). This symmetric zigzag has its bisectrices aligned with the principal directions of $\bar{G}$, which are therefore rotated by an angle ω, presented in the top of Figure S9. Experimental measurements agree well with the theory (shown with continuous lines).

6 Programming axisymmetric shapes

We present here more information about shape programming experiments for inflated fabrics for which $\lambda_\parallel = 1$ and $\lambda_\perp = 0.77$.

We restrict ourselves to symmetric cases where the metric is of the form

$$\bar{G} = \begin{bmatrix} \Lambda_1^2(x_1, x_2) & 0 \\ 0 & \Lambda_2^2(x_1, x_2) \end{bmatrix} \tag{S10}$$

In this particular case where the metric is diagonal, and the area ratio $\Lambda_1 \Lambda_2 = \lambda_\Sigma$ is fixed, the Gaussian curvature reads simply [6, 7]

$$K = \frac{-1}{2\lambda_\Sigma^2} \left(\frac{\partial^2 \Lambda_1^2}{(\partial x_2)^2} + \frac{\partial^2 \Lambda_2^2}{(\partial x_1)^2} \right)$$

and more simply when the zigzag angle only depend on x_2,

$$K = \frac{-1}{2\lambda_\Sigma^2} \frac{d^2 \Lambda_1^2}{(dx_2)^2}$$

We choose to work on strips with height $\mathcal{H}_0$ and length $\mathcal{L}_0$ that are sealed back into a cylinder as in **Figure S10**, and will use

$$\left(\Lambda_1^2\right)'' = -2K\lambda_\perp^2 \tag{S11}$$

to program the Gaussian curvature K.

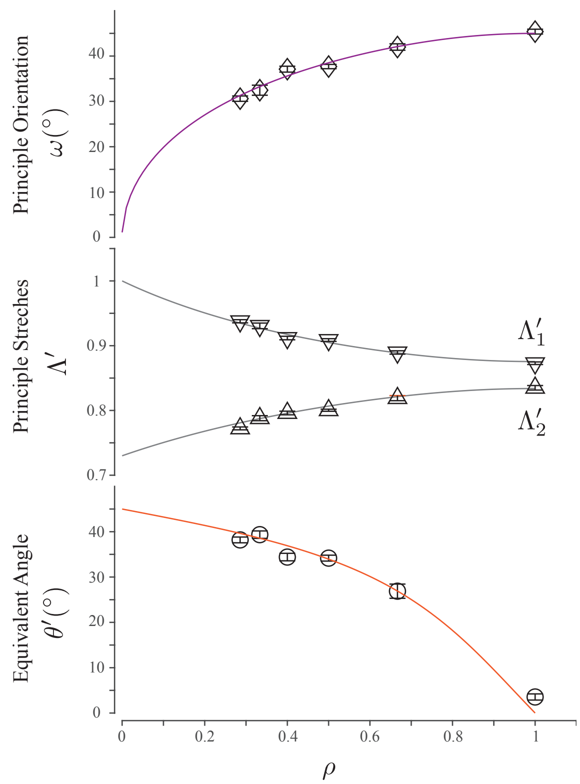

Figure S9: Asymmetric zigzag pattern are equivalent to symmetric zigzag with an orientation rotated by ω (top), and internal angle θ'_0 (bottom). (center) principal stretches (Λ'_1, Λ'_2) as a function of asymmetry parameterρ. Symbols represent experimental measurements with fabrics ($\lambda_\perp = 0.73$ and $\theta_0 = 45°$); theory in continuous line.

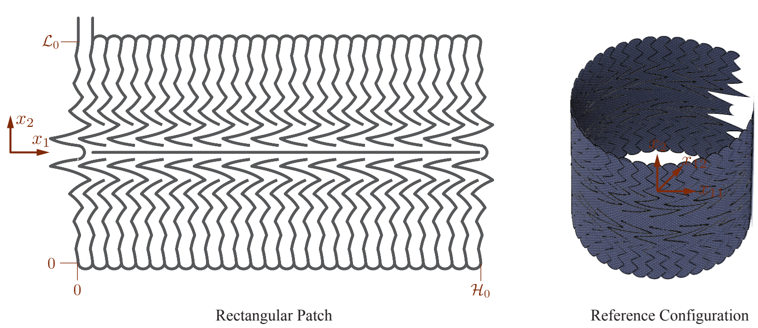

Figure S10: Example of zigzag patterning and ribbon with edges sealed into a tube, before inflation.

6.1 Cones $K = 0$

In the case of a cone with $K = 0$, equation (S11) leads to $[\Lambda_1^2(x_2)]'' = 0$. We wish to program the largest shape change by enforcing $\Lambda_1(0) = 1$ and $\Lambda_1(\mathcal{H}_0) = \lambda_\perp$, so that

$$\Lambda_1(x_2) = \sqrt{\frac{\lambda_\perp^2 - 1}{\mathcal{H}_0} x_2 + 1}$$

In the main text, it is shown that

$$\sin\alpha = \frac{\mathcal{L}_0}{2\pi}\frac{\Lambda_1\Lambda_1'}{\lambda_\Sigma} = \frac{\mathcal{L}_0}{\mathcal{L}_C}$$

where in our case $\mathcal{L}_C = 4\pi\mathcal{H}_0\lambda_\perp/(1-\lambda_\perp^2)$

6.2 Constant non-zero Gaussian curvature K

$\mathcal{L}_0 = 0.5\mathcal{L}_k$ $\mathcal{L}_0 = 0.75\mathcal{L}_k$ $\mathcal{L}_0 = \mathcal{L}_k$ $\mathcal{L}_0 = 1.25\mathcal{L}_k$ $\mathcal{L}_0 = 1.5\mathcal{L}_k$

Figure S11: inflated state woth constant negative Gaussian curvature before gluing into a cylinder take a helical shape (scale bar: 50mm)

We now solve Equation (S11) for constant Gaussian curvature. For positive Gaussian curvature $K > 0$, we aim at the largest curvature by imposing $\Lambda_1(0) = 1$ at the center line of the strip (here noted $x_2 = 0$), and $\Lambda_1(\pm\mathcal{H}_0/2) = \lambda_\perp$ on both edges. We find

$$\Lambda_1^2 = 1 - K_m\lambda_\perp^2 x_2^2,$$

where the maximum Gaussian curvature is

$$K_m = \frac{4}{\mathcal{H}_0^2} \frac{1 - \lambda_\perp^2}{\lambda_\perp^2} = 4 \frac{1 - \lambda_\perp^{-2}}{\mathcal{H}_0^2}$$

For a negative constant Gaussian curvature, we rather impose $\Lambda_1(0) = \lambda_\perp$ and $\Lambda_1(\pm\mathcal{H}_0/2) = 1$, leading to

$$\Lambda_1^2 = \lambda_\perp^2 + K_m \lambda_\perp^2 x_2^2$$

providing the programming for the most negatively curved shells (Gaussian curvature $-K_m$) for such ribbons with height $\mathcal{H}_0$. In **Figure S11** we show the ribbons before sealing them into a cylindrical tube, but inflated. We see that they adopt a helical shapes compatible with uniform negative Gaussian curvature.

6.3 Programming non-constant Gaussian curvature K

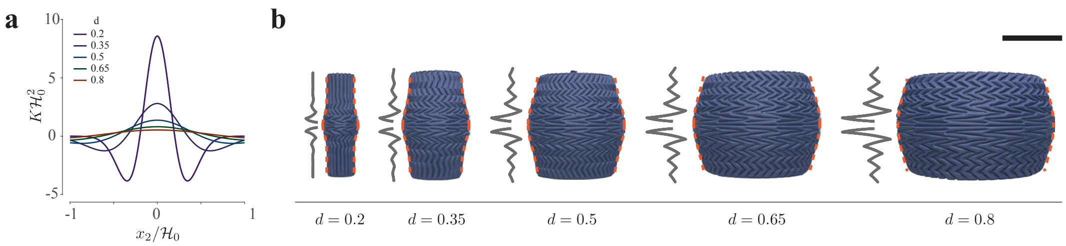

Figure S12: Bulges shapes combining positive and negative Gaussian curvature, obtained from programming in Equation (S12)**.** (a) The programmed Gaussian curvature for different values of d involve positive and negative values. (b) zigzag patterns, experimental pictures and predicted profiles (red doted lines) for different values of parameter d. ($\mathcal{H}_0 = 348; 370; 378; 380; 382$mm we have chosen $\mathcal{L}_0 = 187; 349; 507; 663; 818.5$mm such that the two principal curvature are always equal at the central point $x_2 = 0$.) (scale bar: 100mm)

To further test the capability of our approach, we program bulging shapes corresponding to varying Gaussian curvature, combining positive and negative curvature. One possibility is assigning a stretch function $\Lambda_1^2(x_2)$ that includes positive and negative convexity, see Equation (S11):

$$\Lambda_1^2(x_2) = \lambda_\perp^2 + (1 - \lambda_\perp^2) \exp\left(-\frac{1}{2}\left[\frac{x_2}{d\mathcal{H}_0}\right]^2\right) \tag{S12}$$

where d is a non-dimensional parameter adjusting the profile.

A series of zigzag channels were encoded for serveral values of d (**Figure S12**). As expected, when d is increased, the bulges is less localized. The predicted outlines agree well with experiments.

6.4 Predicting the axisymmetric shape

For all these cases, the axisymmetric shape obeying the metric given by a function $\Lambda_1(x_2)$ is computed numerically with the following procedure.

Axisymmetric shapes are described in cylindrical coordinates as $(r(x_2), z(x_2), \phi)$. The perimeter of a cut at altitude z is $2\pi r(x_2) = 2\pi\Lambda_1(x_2)\mathcal{R}_0$, where $\mathcal{R}_0 = 2\pi\mathcal{L}_0$ is the radius of the initial cylinder, so that

$$r(x_2) = \Lambda_1(x_2)\frac{\mathcal{L}_0}{2\pi} \tag{S13}$$

Examining an element of a meridian cut with length ds leads to

$$dz^2 + dr^2 = ds^2 = \Lambda_2^2 dx_2^2.$$

From these two equations we deduce that

$$\frac{dr}{ds} = \sin\alpha = \pm\frac{\mathcal{R}_0\Lambda_1'}{\Lambda_2} = \pm\frac{\mathcal{L}_0}{2\pi}\frac{\Lambda_1\Lambda_1'}{\lambda_\Sigma}$$

(where α is the orientation of the local tangent to the meridian), so that Equation (6) from the main text holds for any axisymmetric shape. We also obtain

$$\left(\frac{dz}{ds}\right)^2 = 1 - \left(\frac{\mathcal{L}_0}{2\pi}\frac{\Lambda_1\Lambda_1'}{\lambda_\Sigma}\right)^2 \tag{S14}$$

which provides $z(x_2)$ by a simple integration, under the condition that $\mathcal{L}_0 < 2\pi\lambda_\Sigma/(\Lambda_1\Lambda_1')$.

Finally, Equation (S13) and (S14) define the smooth axisymmetric shape $(r(x_2), z(x_2))$ geometrically compatible with the imposed metric distortion, and are used in all the comparison with experimental shapes.

6.5 Design of zigzag patterns with varying angle

Starting from a given distribution $\Lambda_1(x_2)$, the zigzag channels are designed in practice in the following way: From Equation (2) (in main text) we deduce that

$$\sin(\theta_0) = \sqrt{\frac{\lambda_\parallel^2 - \Lambda_1^2}{\lambda_\parallel^2 - \lambda_\perp^2}} = \sqrt{\frac{1-\Lambda_1^2}{1-\lambda_\perp^2}} \tag{S15}$$

and zigzag angle $\theta_0(x_2)$ as a function of x_2.

The actual zigzag seam-line is obtained as

$$Z(x_2) = U(x_2)T(x_2)$$

where $T(x)$ is a symmetric triangle wave with period $P = \mathcal{H}_0/N =$ (with $N = 2$ for a cone, and $N = 4$ for other cases was chosen for practical reason, given the size of the samples) with extremal values ± 1. The amplitude $U(x_2)$ follows

$$U = \frac{P}{4\tan(\theta_0)}$$

and is drawn in pink color in **Figure S13**. The zigzag line $Z(x_2)$ is then offset by steps of d to create the zigzag channels. The distance d is chosen such that everywhere on the pattern the channels are sufficiently elongated (here we have chosen $d = 20$mm). If the seam lines are too far apart, an intermediate seam-line is inserted.

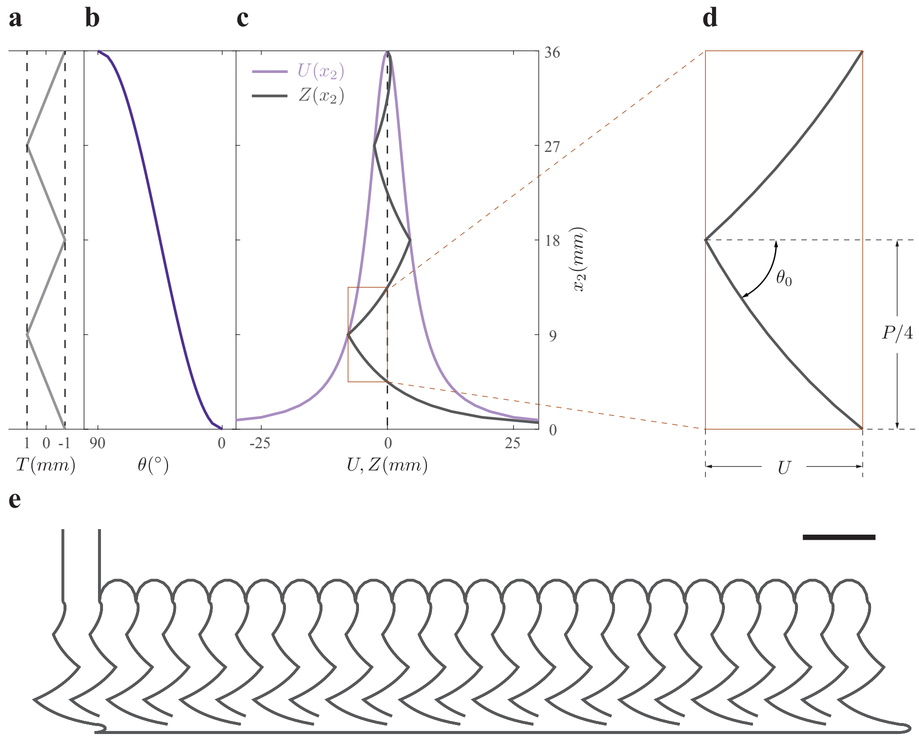

Figure S13: Generation of zigzag pattern on the example of a conical shape. The zigzag in (c) is obtained as the multiplication of a triangle signal (a) with a varying amplitude (c). scale bar: 100mm

References

[1] Emmanuel Siéfert, Etienne Reyssat, José Bico, and Benoît Roman. Programming stiff inflatable shells from planar patterned fabrics. *Soft Matter*, 2020.

[2] E Siéfert, E Reyssat, J Bico, and B Roman. Bio-inspired pneumatic shape-morphing elastomers. *Nature materials*, 18(1):24, 2019.

[3] Jianzhe Gu, David E Breen, Jenny Hu, Lifeng Zhu, Ye Tao, Tyson Van de Zande, Guanyun Wang, Yongjie Jessica Zhang, and Lining Yao. Geodesy: Self-rising 2.5 d tiles by printing along 2d geodesic closed path. In *Proceedings of the 2019 CHI Conference on Human Factors in Computing Systems*, pages 1–10, 2019.

[4] Byoungkwon An, Ye Tao, Jianzhe Gu, Tingyu Cheng, Xiang'Anthony' Chen, Xiaoxiao Zhang, Wei Zhao, Youngwook Do, Shigeo Takahashi, Hsiang-Yun Wu, et al. Thermorph: Democratizing 4d printing of self-folding materials and interfaces. In *Proceedings of the 2018 CHI conference on human factors in computing systems*, pages 1–12, 2018.

[5] M. E. Gurtin. *Introduction to Continuum Mechanics.* Academic Press, 1981.

[6] M. P. do Carmo. *Differential Geometry of curves and surfaces.* Paperback, 1976.

[7] Giancarlo Cicconofri, Marino Arroyo, Giovanni Noselli, and Antonio DeSimone. Morphable structures from unicellular organisms with active, shape-shifting envelopes: Variations on a theme by Gauss. *International Journal of Non-Linear Mechanics*, 118:103278, 2020.